Eurographics/ ACM SIGGRAPH Symposium on Computer Animation (2010)
M. Otaduy and Z. Popovic (Editors)

Constraint-Based Simulation of Adhesive Contact

Jorge Gascón, Javier S. Zurdo & Miguel A. Otaduy

URJC Madrid, Spain

Abstract

Dynamics with contact are often formulated as a constrained optimization problem. This approach allows handling in an integrated manner both non-penetration and frictional constraints. Following developments in the computational mechanics field, we have designed an algorithm for adding the simulation of adhesive contact constraints in the context of state-of-the-art constraint-based contact solvers. We show that implicit adhesion constraints can be handled with minor changes to existing solvers, and we demonstrate our algorithm on a diverse range of objects, including mass-spring cloth, volumetric finite-element models, and rigid bodies.

Categories and Subject Descriptors (according to ACM CCS): I.3.7 [Computer Graphics]: Three Dimensional Graphics and Realism—Animation

1. Introduction

Adhesion can be regarded as a thermodynamic effect in which a potential energy is stored at the interface between two surfaces. Debonding two surfaces that are adhered requires a traction force high enough to release the adhesion energy [RCC99]. In computer graphics, adhesion is commonly handled in the simulation of viscoplastic materials using continuum models (See [BWHT07, WTGT09] for two ways of merging viscoplastic materials due to adhesion).

Instead, in this paper we are interested in modeling and simulating adhesion at a coarser scale, in order to efficiently handle sticking effects at the interface between rigid and/or elastic objects. We follow a constraint-based formulation, inspired by adhesion models described in the computational mechanics literature [Wri02, Fre87, RCC99]. Our main contribution is an algorithm for efficiently handling adhesion as part of constrained dynamics simulation.

Given a constraint-based formulation of contact dynamics (Section 3), and a formulation of adhesion using unilateral constraints (Section 4), we have developed an algorithm (Section 5) for seamlessly integrating adhesion constraints into state-of-the-art constraint-based contact solvers. A priori, this integration is not trivial, because, unlike non-penetration constraints, adhesion constraints are formulated in terms of both contact force and the separation at the contact interface. When formulating these constraints implicitly (a condition for large time steps), they become non-linear, thereby complicating the solution of the system. However, we present an algorithm that elegantly handles implicit adhesion constraints in the context of a projected-Gauss-Seidel solver for linear complementarity problems.

Our approach is general, and it handles rigid bodies, volumetric elastic bodies, thin shells such as cloth, and their combinations, as shown in our examples. Once the mathematical formulation is developed, integrating adhesion in state-of-the-art constraint-based contact solvers is simple and efficient, allowing interesting effects with low effort.

2. Related Work

Constraint-based formulations of contact handling have become popular in computer graphics over the last twenty years [BW92, Bar94, PPG04, KEP05, DDKA06, Erl07, KSJP08, OTSG09, CAR*09]. Most of the existing approaches formulate constrained dynamics as a linear complementarity problem (LCP), which can be solved, for example, using projected-Gauss-Seidel (PGS) relaxation [CPS92]. The benefit of LCP-type solutions is that all constraints are handled simultaneously. Moreover, formulating the constraints implicitly increases robustness under large time steps [ST96], although the constrained problem needs to be linearized in order to cast it as an LCP.

Even though our model is intended to constraint-based simulation of contact, there are also other succesful approaches to contact handling, namely penalty-based meth-

DOI: 10.2312/SCA/SCA10/039-044

Figure 1: *Pieces of candy with diverse adhesion coefficients fall on top of a block of Jell-O.*

ods [BJ07, HVS*09], and impulse-based methods [BFA02, GBF03]. In computer graphics, adhesion (also referred to as *stiction*) has been modeled before in a way similar to penalty forces [JL93, CJY02, BMF03, WGL04, SLF08]. When adhesion takes place, a bilateral spring is set between contact points. As we will discuss later, under traction our adhesion constraints can also be regarded as springs, but under compression they are not active, and we completely enforce non-penetration instead. Another important difference between our constraint-based adhesion and typical adhesive springs is our physically-based model for decohesion.

The formulation of adhesion using constraints was largely developed in the field of contact mechanics by Fremond [Fre87], while Raous et al. [RCC99] developed a thermodynamics background and the connection to friction. A summary can be found in the book of Wriggers [Wri02]. Similar to adhesion, other phenomena, such as puncture [CAR*09], can be modeled using constraints in conjunction with contact.

3. Constraint-Based Contact

In this section, we describe the underlying constrained dynamics formulation where we include the formulation of adhesion constraints. We first describe a general formulation of the constrained dynamics problem, and then we discuss its solution using a PGS solver.

3.1. Formulation

Given state and velocity vectors $\mathbf{q}$ and $\mathbf{v}$ that group the coordinates and velocities of all objects in a scene, we target constrained dynamics formulations of a general form

$$\mathbf{M}\dot{\mathbf{v}} = \mathbf{F}, \tag{1}$$

$$\dot{\mathbf{q}} = \mathbf{G}\mathbf{v}, \tag{2}$$

$$\mathbf{g}(\mathbf{q}) \geq 0. \tag{3}$$

$\mathbf{M}$ denotes de mass matrix and $\mathbf{F}$ is the force vector, $\mathbf{G}$ relates the velocity vector to the derivative of the generalized coordinates ($\mathbf{G}$ is typically identity for deformable bodies, but not for rigid bodies [Sha89]), and $\mathbf{g}$ is a vector of constraints. In our examples, we have used linear co-rotational finite element models [MG04], mass-spring cloth [BFA02], and rigid bodies. We formulate contact constraints by executing continuous collision detection between state updates. The general formulation is valid for other constraints such as joints, although we did not test them in our examples.

We assume that the dynamics equations of the system are discretized and linearized, which yields a constrained velocity formulation of the form:

$$\mathbf{A}\mathbf{v} = \mathbf{J}^T\lambda + \mathbf{b}, \tag{4}$$

$$\mathbf{0} \leq \lambda \perp \mathbf{J}\mathbf{v} \geq \mathbf{c}. \tag{5}$$

The system dynamics may be discretized with explicit integrators or implicit integrators with force linearization (see [BW98] for the formulation of $\mathbf{A}$ and $\mathbf{b}$ under implicit Backward Euler discretization). λ represents contact impulses at the constraints, while Eq. (5) describes non-penetration as linear complementarity constraints. In our examples, we used an implicit position-level LCP, linearized to yield velocity constraints as shown here. This type of formulation (including friction, which is omitted here for readability) can be found, for example, in [DDKA06]. Specifically, we have followed the approach of [OTSG09] for the discretization of both dynamics and contact constraints.

The complete system from Eqs. (4) and (5) constitutes a mixed linear complementarity problem (MLCP). With friction, the system remains an MLCP if friction constraints are expressed using a linearized version of Coulomb's friction cone. We align the friction cone at each contact with the direction of the unconstrained tangential velocity. The MLCP can be transformed into the following LCP:

$$\mathbf{0} \leq \lambda \perp \mathbf{B}\lambda \geq \mathbf{d}, \text{ with} \tag{6}$$

$$\mathbf{B} = \mathbf{J}\mathbf{A}^{-1}\mathbf{J}^T, \quad \mathbf{d} = \mathbf{c} - \mathbf{J}\mathbf{A}^{-1}\mathbf{b}.$$

In our examples, we have used *iterative constraint anticipation* [OTSG09], a variant of this formulation that produces a sparse matrix $\mathbf{B}$ by nesting two relaxation solvers. The approach described in this paper for including adhesive constraints into the LCP is independent of the way in which the LCP is formulated, but, for deformables objects with many degrees of freedom and many contacts, iterative constraint anticipation provides better performance in practice.

The i^{th} constraint in Eq. (6) represents the implicit non-penetration constraint of the i^{th} contact, after linearization and time integration. Then, the gap function g_i at the i^{th} contact at the end of the time step can simply be expressed (up to linearization) as

$$g_i = \Delta t(\mathbf{B}_i\lambda - d_i). \tag{7}$$

$\mathbf{B}_i$ and d_i represent the i^{th} rows of $\mathbf{B}$ and $\mathbf{d}$, respectively.

3.2. Solution

We consider the solution of the LCP problem above using a PGS solver. Then, when a PGS iteration reaches the i^{th} contact, the constraints for that contact can be expressed as:

$$0 \leq \lambda_i \quad \perp \quad B_{ii}\lambda_i - \overline{d}_i \geq 0, \tag{8}$$

$$\text{with } \overline{d}_i = d_i - \overline{\mathbf{B}}_i\overline{\lambda}_i. \tag{9}$$

$\overline{\lambda}_i$ contains all values of λ but λ_i. It combines values from the current iteration of PGS (up to the i^{th} entry), with values from the previous iteration (after the i^{th} entry). $\overline{\mathbf{B}}_i$ is defined accordingly, by removing B_{ii} from $\mathbf{B}_i$.

During each iteration of PGS, the i^{th} contact is handled as follows:

1. Compute $\lambda_i^* = \frac{\overline{d}_i}{B_{ii}}$.
2. Project $\lambda_i = \max(\lambda_i^*, 0)$.

4. Formulation of Adhesion

The thermodynamics model of adhesion by Raous et al. [RCC99] defines an elastic potential energy at a contact interface as a function of the separation gap g and an adhesion intensity β (with both terms squared). The adhesion intensity term captures the thermodynamic effect that, under traction, internal adhesion energy can be released as heat. This thermodynamics model has two implications when developing a computational algorithm for simulating adhesion: (i) it defines a constraint law that relates the maximum adhesive force to the contact gap and the adhesion intensity, and (ii) it defines a physical law for debonding, i.e., the time-dependent reduction of the adhesion intensity due to heat release. In this section, we describe the adhesion constraint law and the debonding law, as well as our own model for bonding, i.e., the time-dependent increase of the adhesion intensity under compression.

4.1. Adhesion Constraints

An adhesion constraint implies that the traction force must be smaller than a maximum defined by the adhesion intensity. Together with the non-penetration constraint, adhesive contact can be formulated with the following complementarity constraints [RCC99, Wri02]:

$$0 \leq -p_i + C_i\beta_i^2 g_i \quad \perp \quad g_i \geq 0, \tag{10}$$

where $\beta_i \in [0,1]$ is the adhesion intensity, C_i is the adhesion stiffness, and p_i is the traction. The value of the adhesion stiffness depends on the materials and the local properties of the contact interface.

In order to handle adhesion in the tangent plane, we use a box model that accounts separately for the normal adhesion and tangential adhesion along two orthogonal directions. We set a local frame on each contact, using the normal $\mathbf{n}$, the direction of unconstrained tangential velocity, $\mathbf{t}$, and the binormal $\mathbf{b} = \mathbf{n} \times \mathbf{t}$. The adhesion constraint can then be expressed for each contact impulse and gap function independently. Tangential adhesion can be regarded as a model similar to Coulomb friction, with the difference that the magnitude of the tangential force is limited by the adhesion intensity, instead of the magnitude of the normal force.

4.2. Bonding

Bonding and debonding model the evolution of the adhesion intensity as a function of the contact traction/compression. In the case of bonding, we account for a bonding rate, r, and a compression value for saturation, p_0. Adhesion intensity will grow as long as compression is exerted, until saturation is reached. Specifically, our bonding model is formulated as:

$$\dot{\beta}_i = r\max(p_i - \beta_i p_0, 0). \tag{11}$$

4.3. Debonding

For the debonding model, we follow the linear case in the thermodynamic adhesion model [RCC99, Wri02]. Considering the adhesion stiffness C and the gap function g, debonding starts taking place once $Cg^2\beta$ reaches a maximum adhesion energy W. The term $Cg^2\beta$ is obtained by differentiating a thermodynamic energy $1/2Cg^2\beta^2$ w.r.t. β. Please see [RCC99] for the full details. During debonding, adhesion decreases at a rate of $\frac{1}{\eta}$, where η is a viscosity parameter. Formally, we can write the debonding model for the i^{th} contact as:

$$\dot{\beta}_i = \frac{1}{\eta}\min(W - C_i g_i^2 \beta_i, 0). \tag{12}$$

5. Algorithm

We describe now our algorithm for including adhesion constraints in the contact solver outlined in Section 3. We start by describing the 1D case, and then extend it to the full 3D case including tangential adhesion. Last, we describe the evolution of the adhesion intensity.

5.1. Implicit Adhesion Constraints: 1D Case

Our goal is to execute a PGS step similar to the one in the non-adhesive case (Eq. (8)). In the adhesion constraint in Eq. (10), contact traction is related to the gap function, hence

implicit adhesion constraints do not allow for a simple computation of a projection value. Contact traction is related to the contact impulse by $p_i = -\frac{\lambda_i}{\Delta t A_i}$, with A_i the local contact area. Accounting for the implicit definition of the gap function from Eq. (7), an adhesion constraint can be reformulated in terms of the contact impulse as:

$$0 \leq \lambda_i + \Delta t A_i C_i \beta_i^2 g_i \quad \perp \quad \mathbf{B}_i \boldsymbol{\lambda} \geq d_i. \tag{13}$$

In order to compute the local area, at edges and vertices we store the averaged area of incident triangles, and at each contact we select the smallest area from those of the two primitives involved in contact. In this way, contact traction is less sensitive to mesh resolution.

By substituting the implicit gap function from Eq. (7), we obtain the following implicit linearized adhesion constraint:

$$0 \leq \lambda_i + \Delta t^2 A_i C_i \beta_i^2 (\mathbf{B}_i \boldsymbol{\lambda} - d_i). \tag{14}$$

A priori, the constraint depends on all values of contact impulses $\boldsymbol{\lambda}$, but we are interested in its evaluation in one PGS step. Then, we can substitute the evaluation of the right-hand-side of the PGS step given by Eq. (9):

$$0 \leq \lambda_i + \Delta t^2 A_i C_i \beta_i^2 (B_{ii} \lambda_i - \overline{d}_i). \tag{15}$$

It suffices to single out λ_i in order to express the implicit adhesion constraint on the contact impulse. By analogy with Eq. (8), in the adhesive case the complementarity constraint in the PGS step turns into:

$$\frac{\Delta t^2 A_i C_i \beta_i^2 \overline{d}_i}{1 + \Delta t^2 A_i C_i \beta_i^2 B_{ii}} \leq \lambda_i \quad \perp \quad B_{ii} \lambda_i - \overline{d}_i \geq 0. \tag{16}$$

As demonstrated, since $\overline{d}_i$ is readily computed during the PGS iteration, applying implicit adhesion constraints effectively reduces to modifying the projection values of the PGS solver.

5.2. Full 3D Adhesion

With the inclusion of tangential adhesion, the contact impulse at the i^{th} contact can be represented as a vector $\boldsymbol{\lambda}_i = (\lambda_{i,n}, \lambda_{i,t}, \lambda_{i,b})^T$, with the tangential impulses aligned with the pre-contact tangent velocity and the binormal. Using a Block-PGS relaxation solver, the $\mathbf{B}_{ii}$ block of the $\mathbf{B}$ matrix is now $\mathbf{B}_{ii} = \begin{pmatrix} B_{ii,nn} & B_{ii,nt} & B_{ii,nb} \\ B_{ii,tn} & B_{ii,tt} & B_{ii,tb} \\ B_{ii,bn} & B_{ii,bt} & B_{ii,bb} \end{pmatrix}$.

By analogy with the case with normal adhesion only, we can write now the implicit normal gap in the case of full 3D adhesion, in the context of the Block-PGS solver:

$$g_{i,n} = \Delta t (B_{ii,nn} \lambda_{i,n} - \overline{d}_{i,n}), \tag{17}$$
$$\text{with } \overline{d}_{i,n} = d_{i,n} - \overline{\mathbf{B}}_{i,n} \overline{\boldsymbol{\lambda}} + B_{ii,nt} \lambda_{i,t} + B_{ii,nb} \lambda_{i,b}.$$

Tangential and binormal gaps can be expressed in a similar way. By inserting these implicit expressions into the adhesion constraints expressed as in Eq. (13), we can single out the contact impulses and formulate the projection values for the Block-PGS solver. At the projection step, tangential and binormal adhesion are handled slightly differently than in the normal direction, because forces must be constrained in positive and negative directions.

Eventually, the algorithm for Block-PGS with implicit adhesive constraints can be outlined as follows:

1. Compute $\overline{d}_{i,n} = d_{i,n} - \overline{\mathbf{B}}_{i,n} \overline{\boldsymbol{\lambda}} + B_{ii,nt} \lambda_{i,t} + B_{ii,nb} \lambda_{i,b}$.
2. Compute $\lambda^*_{i,n} = \frac{\overline{d}_{i,n}}{B_{ii,nn}}$.
3. Project $\lambda_{i,n} = \max(\lambda^*_{i,n}, \min(\frac{\Delta t^2 A_i C_i \beta_i^2 \overline{d}_{i,n}}{1 + \Delta t^2 A_i C_i \beta_i^2 B_{ii,nn}}, 0))$.
4. Compute $\overline{d}_{i,t} = d_{i,t} - \overline{\mathbf{B}}_{i,t} \overline{\boldsymbol{\lambda}} + B_{ii,tn} \lambda_{i,n} + B_{ii,tb} \lambda_{i,b}$.
5. Compute $\lambda^*_{i,t} = \frac{\overline{d}_{i,t}}{B_{ii,tt}}$.
6. If $\lambda^*_{i,t} < 0$, $\lambda_{i,t} = \max(\lambda^*_{i,t}, \min(\frac{\Delta t^2 A_i C_i \beta_i^2 \overline{d}_{i,t}}{1 + \Delta t^2 A_i C_i \beta_i^2 B_{ii,tt}}, 0))$.
7. Else, $\lambda_{i,t} = \min(\lambda^*_{i,t}, \max(\frac{\Delta t^2 A_i C_i \beta_i \overline{d}_{i,t}}{1 + \Delta t^2 A_i C_i \beta_i B_{ii,tt}}, 0))$.
8. Do for $\lambda_{i,b}$ similarly as for $\lambda_{i,t}$.

It is convenient to include a friction model, and, out of tangential adhesion and friction, apply the most restrictive projection. This projection refers to the value used for projection in step 6 above. We have used Coulomb's friction model with a 4-sided pyramid approximation. Same as for tangential adhesion, we align the pyramid in every time step to the unconstrained relative velocity at each contact.

5.3. Adhesion Evolution

After a complete step of the constrained dynamics solve, we evolve the adhesion intensity β at all contacts. First, we determine the compression or traction state, and apply the bonding or debonding model, as appropriate. Normal compression may increase bonding, while normal traction may decrease bonding. Tangential adhesion forces, on the other hand, always tend to decrease bonding (if they exceed the debonding energy). In case of normal traction, we compute the total adhesive traction $p = \|(p_n, p_t, p_b)\|$ and apply the debonding law in Eq. (12). In case of normal compression, we compute the tangential adhesive traction $p = \|(p_t, p_b)\|$, and add simultaneous debonding and bonding effects.

Given the time-derivative of the adhesion intensity, $\dot{\beta}$, we have used a simple explicit Euler integrator in order to compute the adhesion intensity for the next time step. We found that, for our examples, interesting adhesion effects take place with rather slow bonding and debonding dynamics, hence a simple explicit integrator sufficed.

After computing the adhesion coefficient for the next time step, we eliminate contacts where debonding has completely taken place. Eq. (12) models a first order system that never reaches $\beta = 0$, hence we apply full debonding when the gap function at a contact grows beyond a threshold. This threshold is set based on a reference gap value, as discussed next along with our results.

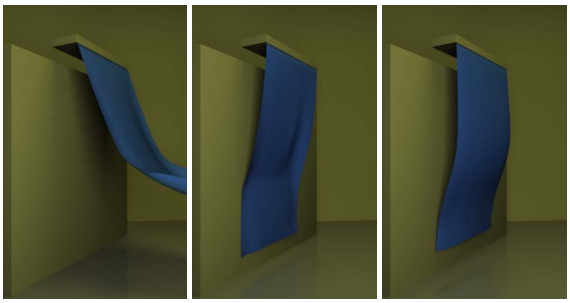

Figure 2: *A swinging cloth hits a wall and adheres to it until it slowly starts debonding.*

Figure 3: *Simulation of an opening and closing mouth, with adhesion taking place at the lips.*

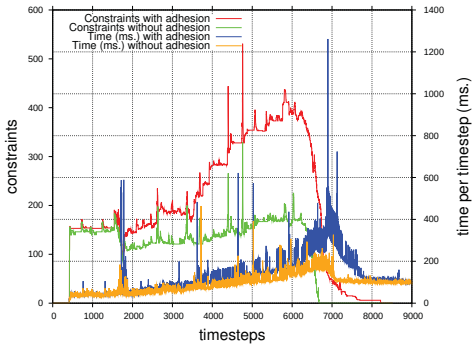

Figure 4: *Comparison of number of contact constraints and timings per timestep for the* candy *demo from Fig. 1 with and without adhesion.*

6. Results

In the accompanying video, we show the behavior of the adhesion model under varying parameter values, and compare it to frictionless contact and friction-only contact. For parameter setting, we used as reference a cube of 10^{-3}m^3 and density 10^3kg/m^3 adhered to the ceiling. This cube produces a traction of 9.8N/m^2. In order to maintain a gap of 1mm under full adhesion $\beta = 1$, the adhesion stiffness must be $C = 10^6$N/m^3. If we assume that debonding takes place at this gap value, then the debonding energy is $W = 1$. The viscosity η can be set based on the desired debonding rate, and similarly the bonding parameters can be set according to the desired bonding rate. In our examples, we have set the gap for full debonding to twice the reference gap. The smaller the reference gap, the larger the required stiffness in order to maintain a certain traction. Thanks to the implicit formulation of adhesion constraints, we were able to simulate in a stable manner adhesion stiffness values in the range of 10^6 to 10^8N/m^3 with time steps between 1ms and 5ms.

Our simulation examples show the application of our algorithm to mass-spring cloth (Fig. 2), and combined rigid and deformable bodies (Fig. 1). In the video of the swinging cloth from Fig. 2, we demonstrate that the overall behavior of adhesion varies little under varying mesh resolution. The *candy* demo depicts rich bonding/debonding effects, and we have also applied our algorithm to a facial animation setting (Fig. 3), where the lips of a character briefly stick to each other when opening the mouth. All our examples were rendered using YafaRay.

We have executed our demos on a 1.8-GHz Intel Core 2 Duo processor PC with 2GB RAM. In the *candy* demo, the deformable objects are meshed with a total of approximately 10K tetrahedra, and the triangle meshes involved in continuous collision detection consist of a total of 28K triangles. The adhesion properties are dominated by the adhesion stiffness of the Jell-O, which is 4×10^7N/m^3, and the Coulomb friction coefficient is $\mu = 0.3$ for all objects in the scene. As shown in Fig. 4, the average number of contacts in the simulation is 151, and a maximum of 531. The 25-second simulation takes 20 minutes to compute (1.6 seconds/frame or 0.4 seconds/timestep with 8ms timesteps), which we consider is reasonably fast for a constrained deformation problem of the size described. We also computed the same simulation without adhesion constraints, and it took 13 minutes (1 second/frame). The main difference for the cost is not the convergence rate, which is almost the same in both cases, but the number of contacts. Without adhesion, contacts break easier, and the average number of contacts is 97, and a maximum of 330, as shown also in Fig. 4.

7. Discussion

In this paper, we have shown a model for adhesive contact that can be efficiently integrated into existing constraint-based contact solvers. It retains the robustness of constraint-based contact while allowing for rich and versatile adhesion effects under a diverse range of object types.

Moreover, the adhesion model incorporates a thermodynamics formulation of debonding from the mechanics literature. Connected to this feature, one limitation in our work is that the formulation of bonding and the connection between friction and adhesion are not sustained by a compa-

rable thermodynamics approach. Regarding friction, we obtained plausible results by selecting the most restrictive constraint out of Coulomb friction and tangential adhesion, as discussed in Section 5.2. Another limitation of our algorithm is that it requires contact tracking, not present in some of the available rigid body dynamics simulators, in order to evolve the value of the adhesion intensity across frames.

Although this was not a major problem in our examples, relaxation solvers, such as Gauss-Seidel, may suffer from slow convergence at times. This is a general limitation in constraint-based contact formulations, and more efficient LCP solvers are still an issue under investigation.

Our model handles only well-defined interfaces between rigid and deformable bodies. Therefore, another interesting extension to our work would be to integrate it with other materials, such as viscoplastic ones, for which adhesion produces very interesting effects.

Acknowledgements

We would like to thank the anonymous reviewers for their comments; Marcos Novalbos, José Miguel Espadero and Pablo Toharia for help with the rendering clusters; Carlos Garre for help with the video; Chari Pérez for a demo concept for the lips; and all the members of the GMRV team at URJC. This work has been funded in part by the Spanish Dept. of Science and Innovation (projects TIN2009-07942 and PSE-300000-2009-5).

References

[Bar94] BARAFF D.: Fast contact force computation for nonpenetrating rigid bodies. *Proc. of ACM SIGGRAPH* (1994). 1

[BFA02] BRIDSON R., FEDKIW R. P., ANDERSON J.: Robust treatment of collisions, contact, and friction for cloth animation. *ACM Transactions on Graphics 21*, 3 (July 2002), 594–603. 2

[BJ07] BARBIČ J., JAMES D.: Time-critical distributed contact for 6-DoF haptic rendering of adaptively sampled reduced deformable models. In *2007 ACM SIGGRAPH / Eurographics Symposium on Computer Animation* (Aug. 2007), pp. 171–180. 2

[BMF03] BRIDSON R., MARINO S., FEDKIW R.: Simulation of clothing with folds and wrinkles. In *2003 ACM SIGGRAPH / Eurographics Symposium on Computer Animation* (Aug. 2003), pp. 28–36. 2

[BW92] BARAFF D., WITKIN A. P.: Dynamic simulation of nonpenetrating flexible bodies. *Proc. of ACM SIGGRAPH* (1992). 1

[BW98] BARAFF D., WITKIN A. P.: Large steps in cloth simulation. *Proc. of ACM SIGGRAPH* (1998). 2

[BWHT07] BARGTEIL A. W., WOJTAN C., HODGINS J. K., TURK G.: A finite element method for animating large viscoplastic flow. *ACM Transactions on Graphics 26*, 3 (July 2007), 16:1–16:8. 1

[CAR*09] CHENTANEZ N., ALTEROVITZ R., RITCHIE D., CHO L., HAUSER K. K., GOLDBERG K., SHEWCHUK J. R., O'BRIEN J. F.: Interactive simulation of surgical needle insertion and steering. *ACM Transactions on Graphics 28*, 3 (July 2009), 88:1–88:10. 1, 2

[CJY02] CHANG J. T., JIN J., YU Y.: A practical model for hair mutual interactions. In *ACM SIGGRAPH Symposium on Computer Animation* (July 2002), pp. 73–80. 2

[CPS92] COTTLE R., PANG J., STONE R.: *The Linear Complementarity Problem*. Academic Press, 1992. 1

[DDKA06] DURIEZ C., DUBOIS F., KHEDDAR A., ANDRIOT C.: Realistic haptic rendering of interacting deformable objects in virtual environments. *Proc. of IEEE TVCG 12*, 1 (2006). 1, 2

[Erl07] ERLEBEN K.: Velocity-based shock propagation for multibody dynamics animation. *ACM Trans. on Graphics 26*, 2 (2007). 1

[Fre87] FREMOND M.: Adherence des solides. *Journal de Mechanique Theorique et Appliquee 6* (1987). 1, 2

[GBF03] GUENDELMAN E., BRIDSON R., FEDKIW R. P.: Nonconvex rigid bodies with stacking. *ACM Transactions on Graphics 22*, 3 (July 2003), 871–878. 2

[HVS*09] HARMON D., VOUGA E., SMITH B., TAMSTORF R., GRINSPUN E.: Asynchronous contact mechanics. *ACM Transactions on Graphics 28*, 3 (July 2009), 87:1–87:12. 2

[JL93] JIMENEZ S., LUCIANI A.: Animation of interacting objects with collisions and prolonged contacts. In *Proc. of the IFIP WG 5.10 Working Conference* (1993), pp. 129–141. 2

[KEP05] KAUFMAN D. M., EDMUNDS T., PAI D. K.: Fast frictional dynamics for rigid bodies. *Proc. of ACM SIGGRAPH* (2005). 1

[KSJP08] KAUFMAN D. M., SUEDA S., JAMES D. L., PAI D. K.: Staggered projections for frictional contact in multibody systems. *Proc. of ACM SIGGRAPH Asia* (2008). 1

[MG04] MÜLLER M., GROSS M.: Interactive virtual materials. *Proc. of Graphics Interface* (2004). 2

[OTSG09] OTADUY M. A., TAMSTORF R., STEINEMANN D., GROSS M.: Implicit contact handling for deformable objects. *Computer Graphics Forum 28*, 2 (Apr. 2009), 559–568. 1, 2

[PPG04] PAULY M., PAI D. K., GUIBAS L. J.: Quasi-rigid objects in contact. *Proc. of ACM SIGGRAPH/Eurographics Symposium on Computer Animation* (2004). 1

[RCC99] RAOUS M., CANGÉMI L., COCU M.: A consistent model coupling adhesion, friction, and unilateral contact. *Computer Methods in Applied Mechanics and Engineering 177*, 3-4 (1999). 1, 2, 3

[Sha89] SHABANA A. A.: *Dynamics of Multibody Systems*. John Wiley and Sons, 1989. 2

[SLF08] SELLE A., LENTINE M., FEDKIW R.: A mass spring model for hair simulation. *ACM Transactions on Graphics 27*, 3 (Aug. 2008), 64:1–64:11. 2

[ST96] STEWART D. E., TRINKLE J. C.: An implicit time-stepping scheme for rigid body dynamics with inelastic collsions and Coulomb friction. *International Journal of Numerical Methods in Engineering 39* (1996). 1

[WGL04] WARD K., GALOPPO N., LIN M. C.: Modeling hair influenced by water and styling products. In *Proc. of Computer Animation and Social Agents (CASA)* (2004), pp. 207–214. 2

[Wri02] WRIGGERS P.: *Computational Contact Mechanics*. Wiley, 2002. 1, 2, 3

[WTGT09] WOJTAN C., THÜREY N., GROSS M., TURK G.: Deforming meshes that split and merge. *ACM Transactions on Graphics 28*, 3 (July 2009), 76:1–76:10. 1